# DEVELOPMENT OF PROGNOSTICS TECHNIQUES FOR SURFACE DEFECT GROWTH IN RAILROAD BEARING ROLLING ELEMENTS

A Thesis

by

NANCY DE LOS SANTOS

Submitted to the Graduate College of
The University of Texas Rio Grande Valley
In partial fulfillment of the requirements for the degree of

MASTER OF SCIENCE IN ENGINEERING

July 2019

Major Subject: Mechanical Engineering

# DEVELOPMENT OF PROGNOSTICS TECHNIQUES FOR SURFACE DEFECT GROWTH IN RAILROAD BEARING ROLLING ELEMENTS

A Thesis
by
NANCY DE LOS SANTOS

COMMITTEE MEMBERS

Dr. Constantine Tarawneh
Chair of Committee

Dr. Robert Jones
Co-Chair of Committee

Dr. Arturo Fuentes
Committee Member

July 2019

ABSTRACT

De Los Santos, Nancy, Development of Prognostic Techniques for Surface Defect Growth in Railroad Bearing Rolling Elements. Master of Science in Engineering (MSE), July, 2019, 44 pp., 2 tables, 19 figures, 18 references

One of the major causes of failure in railroad bearings used in freight service is rolling contact fatigue (RCF). RCF is due to subsurface inclusions which are a result from impurities in the steel that is used to fabricate the bearings. Once the bearings initiate subsurface fatigue cracks, they will then propagate upward and initiate spalling of the rolling surfaces. These spalls will begin small and continuously propagate with operation as this induces additional crack forming and spalling. Studies have indicated that bearing temperature is not a good indicator of spall initiation. In many cases, the temperature of the bearing increases markedly once the spall has propagated across major portions of the raceway. However, vibration signatures can be used to detect spall initiation and can track spall deterioration. No monitoring system technique can indicate the growth rate of a spall nor can it determine the bearing residual useful life. Therefore, the principle objective of this study is to develop reliable prognostic models for spall growth within railroad bearings that are based on actual service life testing rather than theoretical simulations. The data used to develop the models presented in this study have been acquired from laboratory and field testing that initiated in 2010. The growth models in this study are for spalls that initiated on the bearing inner (cone) and outer (cup) rings. Coupling these prognostic

models with a vibration-based bearing condition-monitoring algorithm previously developed, will provide the rail industry with an efficient tool that can be used to propose proactive maintenance schedules that will reduce unnecessary and costly train stoppages and delays and will prevent catastrophic derailments.

## DISCLAMER

The contents of this thesis reflect the views of the authors, who are responsible for the facts and the accuracy of the information presented herein. This document is disseminated under the sponsorship of the U.S. Department of Transportation's University Transportation Centers Program, in the interest of information exchange. The U.S. Government assumes no liability for the contents or use thereof.

# DEDICATION

I would like to dedicate this thesis to my loving family. My parents Jose Luis De Los Santos and Bertha Alicia De Los Santos for their unconditional love and support. Thank you for constantly reminding me that education is the key to success. This would not be possible without the guidance, devotion and sacrifice of your hard work. To my sisters Maria and Janet and to my cousin Jorge who made getting this education possible through non-stop support.

Me gustaría dedicarle esta tesis a mi amada familia. A mis padres José Luis De Los Santos y a Bertha Alicia De Los Santos por su amor y apoyo incondicional. Gracias por recordarme constantemente que la educación es la llave del éxito. Esto no sería posible sin la guianza, devoción y el sacrificio de su arduo trabajo. Para mis hermanas María y Janet y para mi primo Jorge quienes hicieron posible esta educación por medio de su apoyo.

ACKNOWLEDGEMENTS

I would like to thank Dr. Constantine Tarawneh for giving me the opportunity to join his research team when no other professor gave me a chance. Thank you for always believing in me even when I gave you no reason to do so. Through your mentorship I was able to develop as an engineer in ways I never imagined. I was able to publish papers, present in conferences, get a fellowship and even participate in co-ops. You were the reason why I pursued a master's degree and for that I am forever grateful.

Dr. Robert Jones, thank you for motivating and challenging me to become a better presenter and student. Your guidance has given me the confidence to excel as an engineer.

Dr. Arturo Fuentes, thank you for always being available when I needed help with my project, your insight helped tremendously in the initial stages of this thesis.

A special thanks to the University Transportation Center for Railway Safety (UTCRS) for their support on this project, each and every one of you helped make this possible. Especially, Jennifer Lima for her willingness to help me out in the laboratory, gathering data and for covering for me when I was away.

Finally, this study was made possible by funding provided by The University Transportation Center for Railway Safety (UTCRS), through a USDOT Grant No. #DTRT 13-G-UTC59

TABLE OF CONTENTS

Page

LIST OF TABLES

Page

LIST OF FIGURES

Page

# CHAPTER I

## BACKGROUND & INTRODUCTION

Freight railcars carry heavy loads that are distributed equally among eight tapered roller bearings that are positioned at the ends of wheel-axle assemblies. A typical freight railcar tapered-roller bearing as shown in Figure 1, has one outer ring (cup) and two inner rings (cones) with rollers that transfer the load between the cup and the cones. The outer ring is supported on one side by the railcar side frame. The load path of the railcar travels from the side frame through the bearing adapter and from there to the bearing cup, the bearing cup then transfers the load to the cones through the rollers.

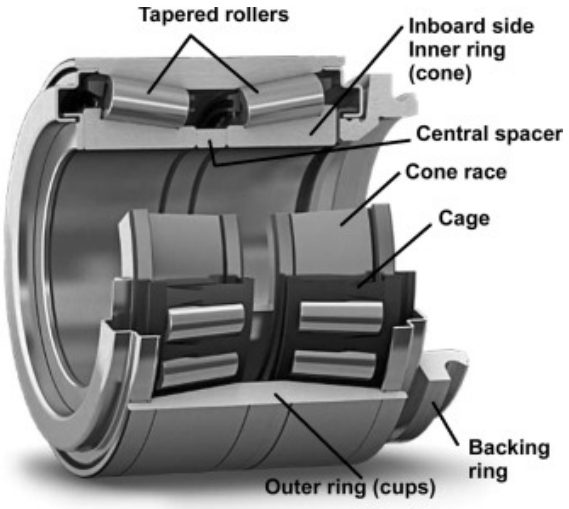


Figure 1. Typical railroad tapered-roller bearing assembly [1]

The outer ring (cup) does not rotate during operation unless the bearing indexes slightly during service. Indexing occurs when the railcar wheels hit a bump in the rail tracks causing the side frame to momentarily lose contact with the bearing adapter. When the railcar operates under normal bearing conditions, the upper 'hemisphere' of the outer ring is always loaded, therefore, it is referred to as the 'loaded zone', while the bottom 'hemisphere' is referred to as the 'unloaded zone', as shown in Figure 2. Unlike the cups, which are fixed, the inner rings (cones) are simultaneously rotating with the wheel and axle undergoing cyclical loading and unloading as they enter and exit the loaded and unloaded zones [2].

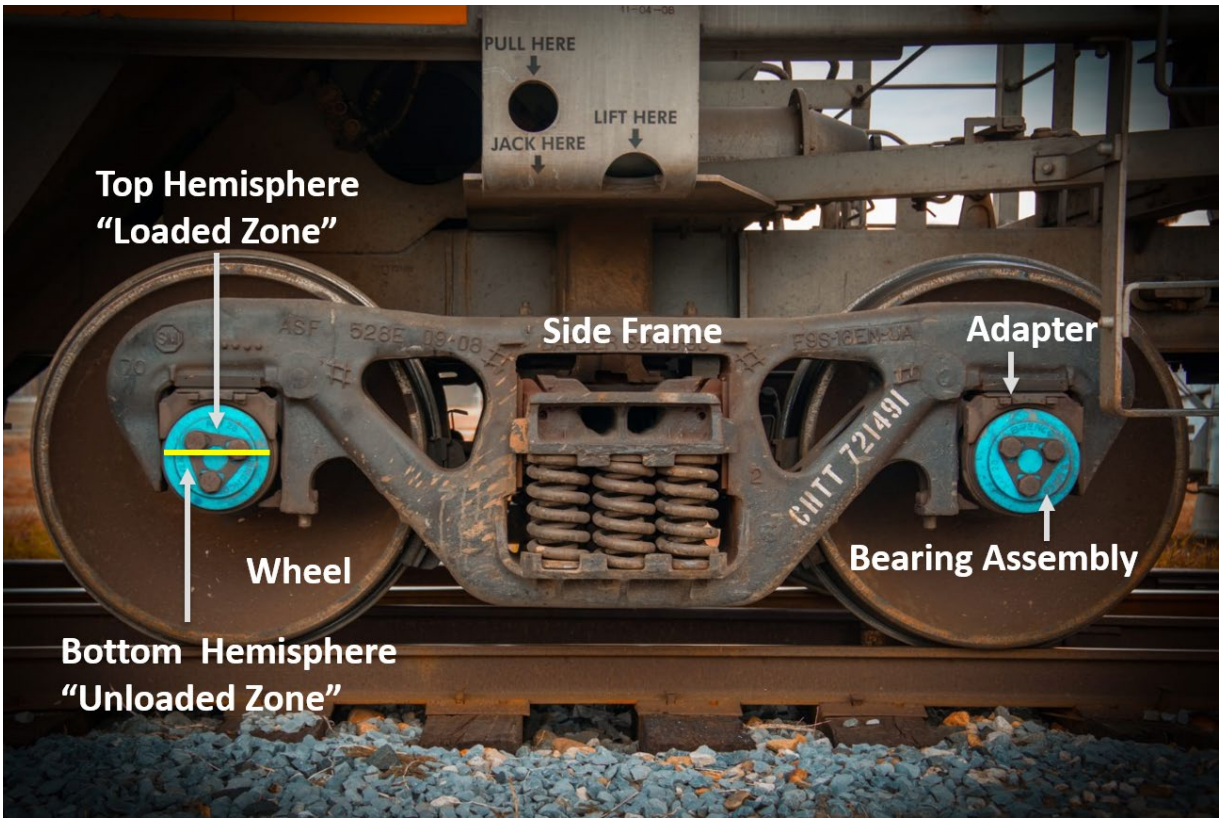


Figure 2. Railcar assembly

A common cause of railroad tapered-roller bearing failure is due to rolling contact fatigue (RCF) which leads to spalling of the cup or cone raceways [2-4]. According to Hertzian contact mechanics theory, the highest shear stresses occur 200-600 μm below the rolling surface [2-4]. The presence of impurities in the steel within the subsurface region can cause local stress levels in these areas to reach values that exceed the endurance limit of the steel, which result in micro-cracking to initiate around the subsurface inclusions. Continuous operation will cause the micro-cracks to propagate until reaching the raceway surface, causing parts of the metal to break off and creating what is known as a 'spall' [4-7]. When spalling initiates on the bearing raceways it usually is accompanied by metallic debris that is introduced to the bearing's lubricant as well as the dynamic components. The buildup of debris during operation can cause the bearing to have high pressure spikes as the rollers continue to run along the inner and outer ring raceways. This causes further deterioration to both raceways [6]. The pitting of the rolling surface in conjunction with the debris buildup may result in additional and more significant misalignment of the rollers as they enter the bearing loaded zone this effect can impact the rollers to a certain extent. Roller misalignment leads to an increase in frictional heating as the rollers slide against the raceway rather than rotate. This effect causes higher operating temperatures and can possibly accelerate the breakdown of the lubricant [6-8]. Laboratory testing has demonstrated that continuous operation of the bearing after initial spalling will result in the spall growing over time [8]. The work presented in this thesis investigates the actual growth rates in bearing inner (cones) and outer (cups) rings that experienced spalling during field and/or laboratory service operation.

Note that railroad bearing empirical prognostic models have not been well-developed because of the highly stochastic nature of the railroad bearing fatigue process. Even though

rolling contact fatigue (RCF) is an area of study that many researchers are actively working on, the majority of the work has been focused on ball bearings and gears used for turbines and other machinery [3, 6, 7, 9-12], and not railroad tapered roller bearings. Furthermore, these studies had minimal experimental validation due to mainly studying the theoretical and analytical models that predict crack propagation and contact fatigue. In contrast to these studies, the data collected for this thesis reflects nine years of laboratory testing under simulated service with varying loads, speeds and bearing temperatures. This research is ongoing at the University Transportation Center for Railway Safety (UTCRS), where the research team continues to track the spall defect growth in several bearing inner and outer rings. Other related work presents a dynamic prognostic prediction of defect propagation on rolling element bearings which modeled general rolling element bearings for machinery [9]. The model presented successfully predicted the growth of a manufactured spall that was symmetrically located. However, this study differs in that it is focused on freight railroad bearings with original spalls that developed naturally during service. In this study, prediction of the remaining life is derived from spall growth as a function of the total distance of operation since this is the standard industry measure. The data presented in this study represents a population of spalls monitored over a prolonged period of operation, with the purpose of establishing with a high degree of confidence, bounding rates of growth for spalls independent of spall location and operating speed, load, and temperature. Previous work had been done to rule out spall growth based on load, speed and temperature during operation.

The work in this thesis is organized as follows: Chapter 2 presents the experimental procedures and testing setup. Chapter 3 presents the spall mapping methodology performed in bearings that undergo, testing, casting impressions and measurements for record keeping. In

Chapter 4, a detailed discussion of the laboratory results obtained from the testing is provided. Prognostic correlations that relate spall growth rates to total distance traveled are also presented in Chapter 4 along with examples of how these correlations are applied to determine remaining service life of bearings. Finally, Chapter 5 gives a summary of the main conclusions from this work.

# CHAPTER II

# EXPERIMENTAL SETUP AND PROCEDURES

## 2.1 Bearing Class Selection for Laboratory Testing

The Association of American Railroad (AAR) has four bearing classes that are commonly used in the United States and Canada for freight trains. The four classes of bearings are class F, class K, class G and class E railroad tapered-roller bearings. The data in this thesis was collected through the testing of class K (6 ½"× 9") and class F (6 ½"× 12") roller bearings since these two classes of bearings are interchangeable and are widely used in the freight rail transportation in the United States and Canada. Class F and class K railroad bearings account for 90% of the entire bearing population used in freight rail in the U.S. and Canada, this is followed by class E with 6% and class G with 4%. This data was provided by two of the largest railroad manufacturing industries in the United States. A visual representation of both class K and F are shown in Figure 2.

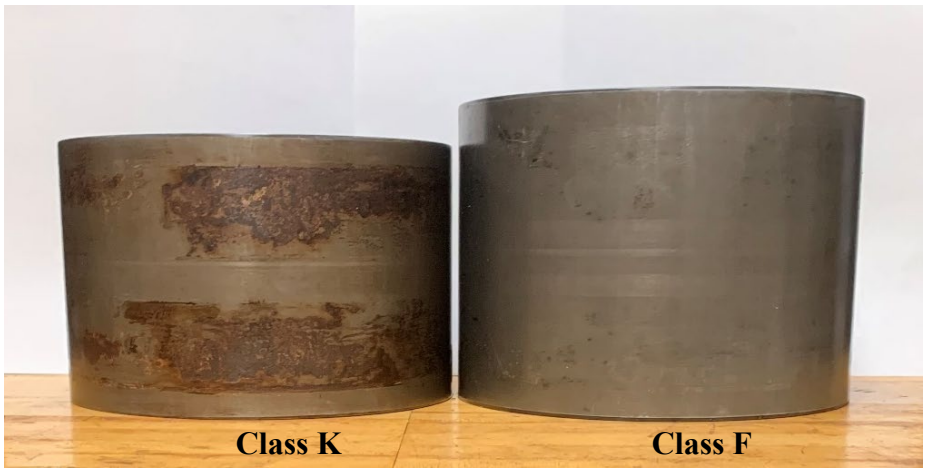


Figure 3. Comparison of class K and class F cups (outer rings)

Class F and class K bearings are fabricated out of AISI 8620 steel with the tapered-rollers being case-hardened. Railroad bearing manufacturers emphasize the use of the highest quality steel with minimal inclusions. The main components for class K and class F bearings have the same dimensions except for the spacer ring width in a class K bearing being 1.46 to 1.48 cm (0.575 to 0.5825 in), whereas, the spacer width for a class F bearing is 3.68 to 3.94 cm (1.45 to 1.55 in). The latter differences make the width of the class K bearing outer ring (cup) roughly 2.34 cm (0.92 in), on average, shorter than the corresponding class F bearing cup. Since the gap between the two inner cone assemblies is smaller in a class K bearing, the manufacturer recommends that the two cone assemblies be properly lubricated, however, no grease should be placed in the spacer region. Table 1 denotes the amount of grease distribution per bearing for both class K and class F.

Table 1. Grease measurements for class K and class F bearings

| Bearing Class | Total Amount of Lubricating Grease | Lubricating Grease on Spacer Region | Lubricating Grease on cone Assemblies |
|---|---|---|---|
| Class F | 0.6506 L (22 oz) | 0.2661 L (9 oz) | 0.3845 L (13 oz) |
| Class K | 0.3845 L (13 oz) | N/A | 0.3845 L (13 oz) |

It is important to know that class K bearings were designed to replace class F bearings since 2001 yet many class F bearings are still in operation. The latter is the reason why this thesis contains both classes of bearings. Ongoing testing and performance characterization of both classes of bearings since 2005 have concluded that there are no noticeable differences in the thermal and dynamic performance of these two bearings.

## 2.2 Laboratory Test Setup

The laboratory testing for this thesis was carried out using railroad bearing dynamic test rigs that closely mimic field service conditions. Two types of test rigs are available, one is a four bearing tester and the other is a single bearing test rig. Both testers are driven by large 22.3 kW (30 hp) variable speed motors that provide rotational speeds equivalent to train velocities of 8 to 137 km/h (5 to 85 mph). Identical hydraulic cylinders were used in both testers. The hydraulic cylinder can apply a maximum load that is equivalent to 150% of the full-load of a class F or class K bearing. Note that 100% load (full-load) for both class F and K bearings is equivalent to 153 kN (34.4 kips), as established by the Association of American Railroads (AAR), whereas, an

empty railcar load is approximately 17% of the full load or 26 kN (5.85 kips) for class F and K bearings.

### 2.2.1 Single Bearing Tester Rig

The single bearing tester (SBT) of Figure 4 can apply vertical, impact, and lateral loads to the railroad bearing in order to closely mimic normal and abnormal operating conditions. The SBT can provide maximum lateral loads of up to 22 kN (5 kips) and maximum vertical loads of up to 222 kN (50 kips). To prevent the tester's support bearings from overheating during testing operations, a cooling system was fabricated and incorporated. The system runs chilled water over the pillow blocks which house the support bearings. Aside from the cooling system, the tester also has two industrial-strength fans that simulate field service conditions. These fans provide an airflow of 23.4 km/h (14.5 mph) across the bearing's outer ring. The single bearing tester was designed to facilitate easier mounting and removal of the bearing from the axle without the need to remove the axle from the test rig. This tester design allows for more frequent teardowns of the test bearing, which is why this tester is utilized to run bearings with defect sizes greater that 6.45 $cm^2$ ($1in^2$) for cones and 12.9 $cm^2$ (2 $in^2$) for cups. Defects of this size or larger require very close tracking of the spall area with operating distance.

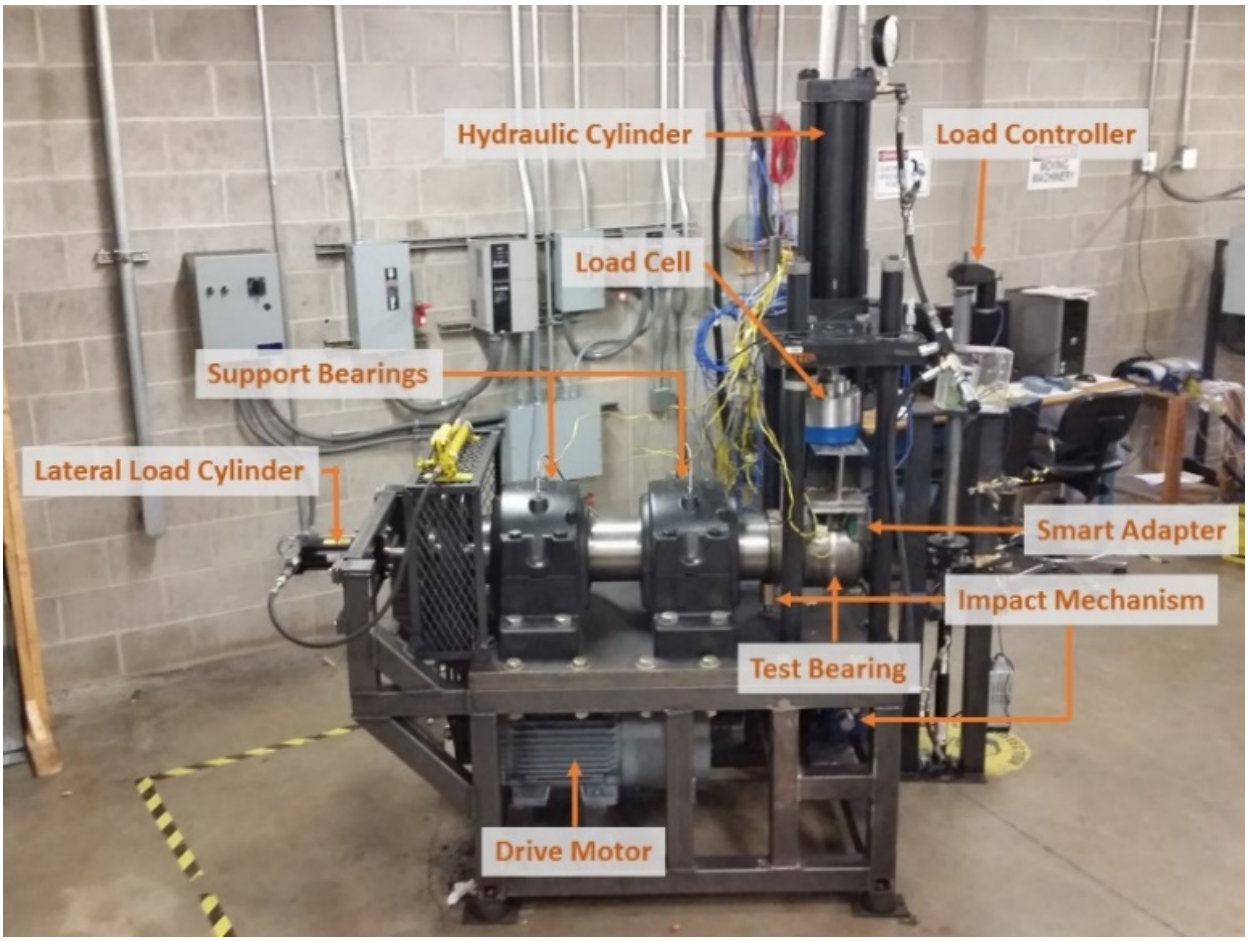


Figure 4. Single bearing tester (SBT)

### 2.2.2 Four Bearing Tester Rig

The four-bearing test rig (4BT) pictured in Figure 5 accommodates four bearings of either class K or class F. The 4BT was designed for long duration testing termed service life testing. Bearings are run continuously at a designated load and speed for months at a time. To simulate real service operations, the test bearings are always placed in the middle two spots, which are the locations where the bearings are top loaded as is the case in field service operations. The outer two bearings, which are bottom loaded, are healthy (defect-free) control bearings. The 4BT rig is housed in an environmental chamber that can simulate ambient

temperatures as low as -40°C (-40°F) and as high as 60°C (140°F). Just like the SBT, the 4BT also has industrial-strength fans that direct airflow over the bearings.

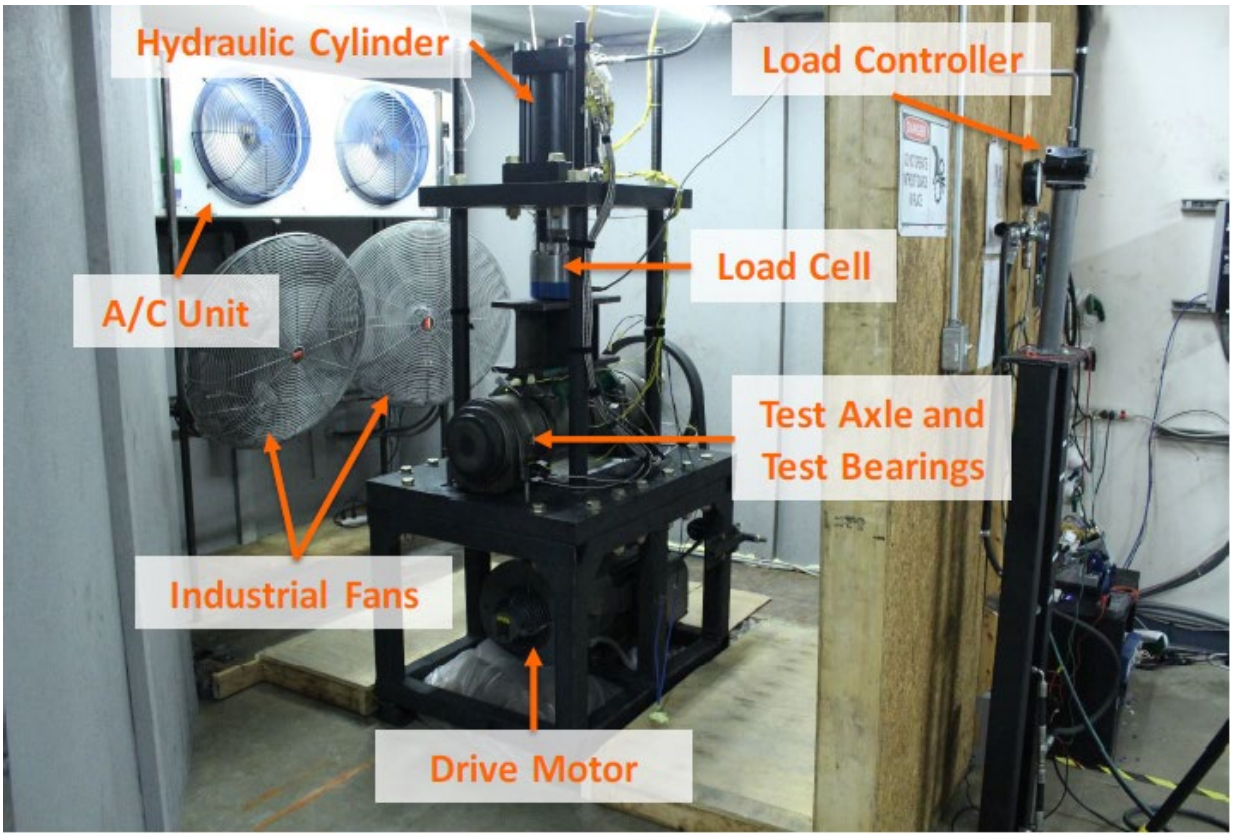


Figure 5. Four-bearing test rig housed within an environmental chamber that can simulate ambient temperatures of -40°C to 60°C (-40°F to 140°F)

### 2.2.3 Data Acquisition

A National Instruments (NI) cDAQ-9174 data acquisition system (DAQ) programmed using the engineering software LabVIEW™ was utilized to monitor and log the temperature and vibration signatures of the test bearings collected using K-type thermocouples and accelerometers, respectively as shown in Figures 6 and Figure 7. The K-type thermocouples were connected to the NI 9213 temperature card of the DAQ, whereas, the accelerometers were

connected to a combination of 8-channel NI 9239, a NI USB-6008, and a NI 9234 cards via 10-32 coaxial jacks and BNC connections. The temperature data were acquired at a sampling rate of 128 Hz once every 20 seconds, whereas, the vibration data was acquired at a sampling rate of 5120 Hz for four seconds at ten-minute intervals.

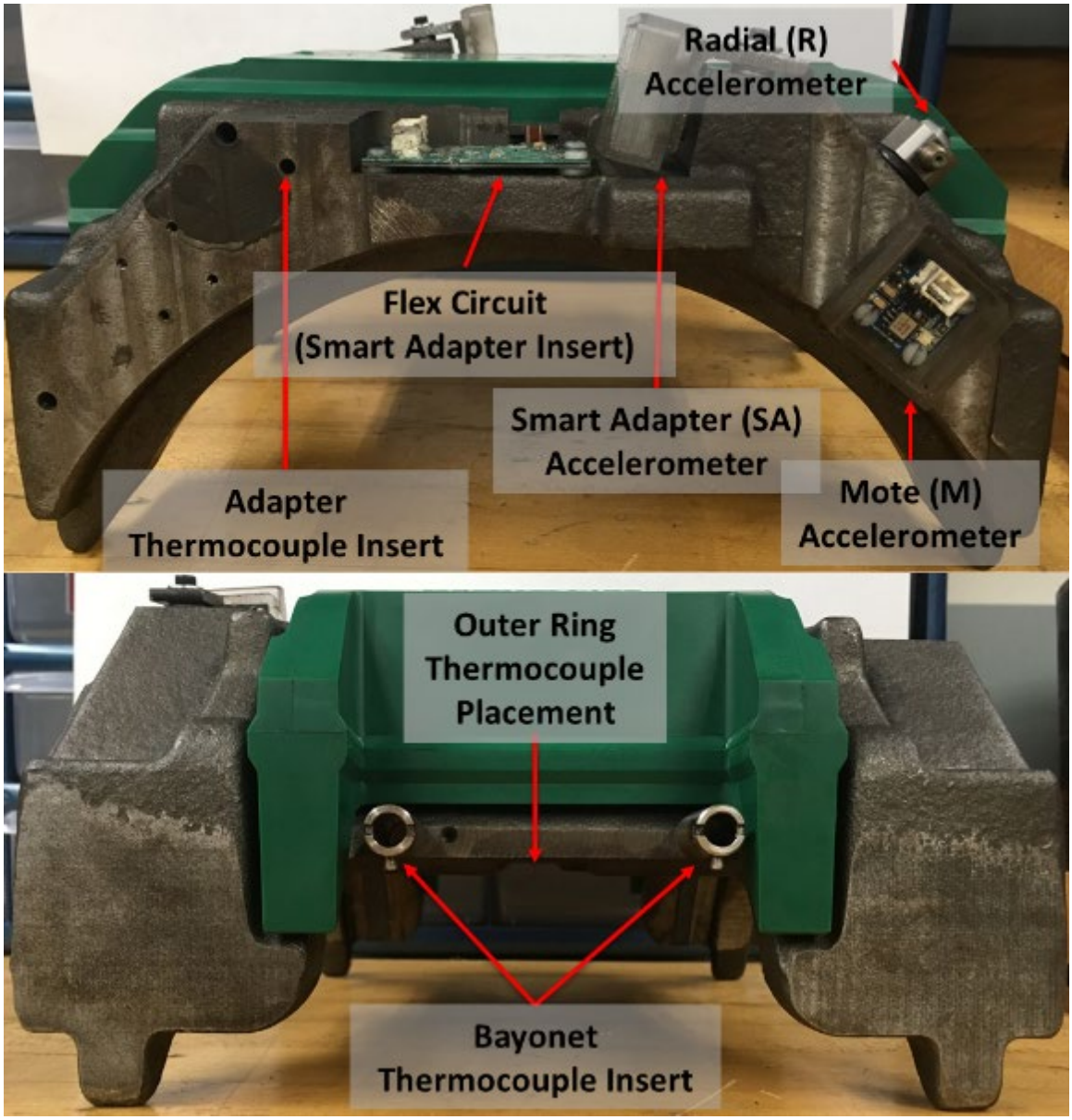


Figure 6. Accelerometers and thermocouple mounting locations on the bearing adapter

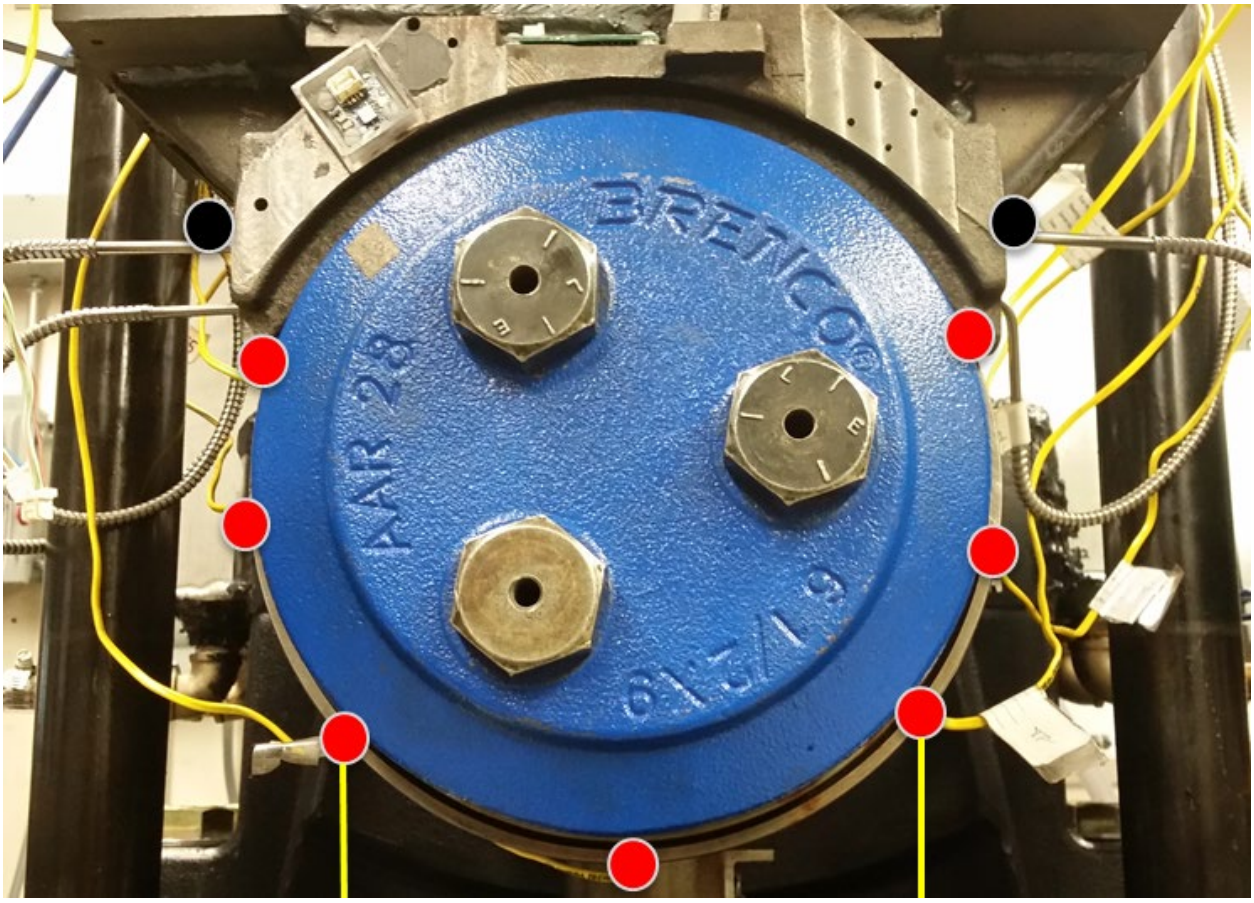


Figure 7. Placement locations for thermocouples on the outer ring (red) and on the bearing adapter (black)

# CHAPTER III

## SPALL MAPPING METHODOLOGY

The spall data used in this thesis came from two different sources; namely, service life testing of bearings with subsurface inclusions on the inner (cone) or outer (cup) rings [2, 4, 5, 14] and bearings that were removed from service due to having a spall on one of the cones (inner rings) or the bearing cup (outer ring) when inspected [8]. For the service life testing data, new defect-free bearings were selected by the manufacturer and ultrasonically scanned to indicate any subsurface inclusions within 600 μm from the rolling surfaces of the cones and the cups [2, 4, 5]. The bearings in the latter three references were run on the 4BT pictured in Figure 5 until spalls were developed during the service life test. Therefore, proper documentation of the exact distance traveled to when the bearings initiated the spall(s) is documented. As per the bearings with spalls removed from field service, the distance traveled leading to these spall sizes is unknown. Though the distance traveled to spalling cannot be tracked, it is important to note that these bearings did not seize in operation nor did they trigger any wayside detectors. These bearings were removed from operation due to defective wheels and upon teardown and inspection were found to have spall(s) less than 6.45 $cm^2$ ($1in^2$) in total area on the inner or outer ring of the bearing. To ensure that both sets of data can be used in this analysis, the prognostic models developed in this thesis are not a function of the distance traveled leading to the spall initiation, but rather the distance traveled after the initial spall(s) have developed.

For this thesis, a total of 23 bearings were used, 20 of which were new bearings that underwent ultrasonic scanning by the bearing manufacturer and were found to have subsurface inclusions on nine inner rings and 11 outer rings. The other three bearings were removed from service and were found to have spalls on two outer rings and one inner ring. Even though only 23 total bearings were tested over the past nine-year period starting in 2010, some of these bearings were run for several iterations over extended periods of time which allowed the growth of the developed spalls to be tracked with distance traveled generating multiple data points for each bearing tested.

Service life testing typically requires new bearings to run for an equivalent distance of 402,325 km (250,000 mi). In a service life test, two bearings can be tested simultaneously on the four-bearing tester (4BT) and the duration of each service life test is about five months assuming no delays or interruptions in testing occur. To accelerate testing and to ensure worst-case operating conditions, both testers were run at 137 km/h (85 mph) and full load of 153 kN or 34.4 kips per bearing for most of the testing period. Lower running speeds and loads that simulate an empty railcar (17% of full-load) were utilized briefly at the beginning of each test, which allowed the lubricant to break in slowly and avoid sudden overheating of the bearings. As part of the experimental setup, regions of the outer ring (cup) containing the worst subsurface inclusions were clearly marked and placed directly under the full-load path (top center) [2]. In the case of the bearing cups that already contained spalls, the spalled region was placed directly under the full-load path.

Testing typically initiates on the Four Bearing Tester (4BT) which accommodates two top-loaded test bearings per experiment. These experiments are run until the bearings develop spall defects. Once the spall area has reached a measurement of 6.45 $cm^2$ (1 $in^2$) for cones and 12.9 $cm^2$ (2 $in^2$) for cups, the bearing is then moved to the Single Bearing Tester (SBT) which can facilitate frequent teardowns and inspections. If the two test bearings placed on the 4BT both contain spalls, the bearings are pressed onto the test axle in a manner that ensures that these spalls are as far away from each other as possible to minimize cross-talk in the accelerometers.

For over a decade now, the University Transportation Center for Railway Safety (UTCRS) at the University of Texas Rio Grande Valley (UTRGV) has been collecting vibration, load, and temperature data from healthy (defect-free) and defective bearings that were run under various combinations of speed and load. These experiments were conducted using the test rigs shown in Figure 4 and Figure 5. A previous study by the UTCRS was conducted summarizing the average operating temperatures of healthy and defective bearings for speeds ranging from 40 km/h (25 mph) to 137 km/h (85 mph) and loads simulating an empty railcar (17% of full-load) and a fully-loaded railcar (100% load corresponding to 153 kN or 34.4 kips per bearing) [15]. The defective bearings used in that study mostly consisted of spalls located on the raceways of either cups or cones. The laboratory data acquired for the temperature, load, and vibration in conjunction with the field test data have been used to develop an advanced bearing health monitoring algorithm [16, 17].

### 3.1. Algorithm

The developed algorithm has proven to detect, with a 95% confidence level, the initiation of the defect as well as the progression in the inner ring (cone) and outer ring (cup) raceways [16]. The algorithm can differentiate between a spall located on the cone raceway and one located on the cup raceway, as well as the approximate size of the defect (within 10%). This algorithm utilizes the vibration signature of a bearing as captured by the onboard accelerometers to track the initiation of the spall and its propagation. Once the bearing condition-monitoring algorithm signals a defect or a spall propagation in one of the bearing components, the bearings are pressed off the testing axle and disassembled for visual inspection of all the bearing components. This teardown procedure is also done every 96,560 km (60,000 mi) of continuous un-interrupted operation even when the algorithm has not detected any defects or spall propagation. This process was implemented to ensure that there are no defects that have developed or deteriorated without the algorithm detecting these events first.

### 3.2 Spall Casting

After each teardown procedure, the bearings are disassembled to conduct a thorough visual inspection. The bearings are properly cleaned out and a visual inspection is preformed of all the components (see Figure 1 for details on bearing components). In order to maintain a dependable record of any spall formation and/or progression while still allowing continuous testing of the spalled bearing, a casting of the defect (spall) area was created. Castings are done using low-melting, zero-shrinkage Bismuth alloy which has a melting point of 80°C (176°F). The castings are done by enclosing the spall region with tacky tape that has a melting point of 204°C (400°F), then pouring the molten Bismuth alloy into the frame surrounding the defect area created by the tacky tape, as demonstrated in Figure 8. Once the bismuth has cooled and

hardened, the casting is removed and painted to enhance the contrast of the defect against the rest of the molding. The painted spall casting is then photographed, and an image is uploaded to the mathematical software MatLab™, which is used to render a monochromatic image of the casting, as shown in Figure 9. This image was further analyzed using Image-Pro®Plus, a specialized image software that was used to measure the exact spall size, as depicted in Figure 9. This software outputs an Excel sheet with measurements that include the area, length, and width of the spall (defect). The values obtained from this software are then entered in a spreadsheet where all the inner (cone) and outer (cup) ring raceway defect data is compiled. This compiled spall area data is then compared to its associated vibration data to further improve the accuracy of the bearing condition monitoring algorithm in terms of prognostics on the spall size and its growth based on vibration levels within the bearing.

Figure 8. A picture demonstrating the casting procedure using Bismuth; (left) spalled surface outlined with tacky tape; (right) Bismuth alloy cast

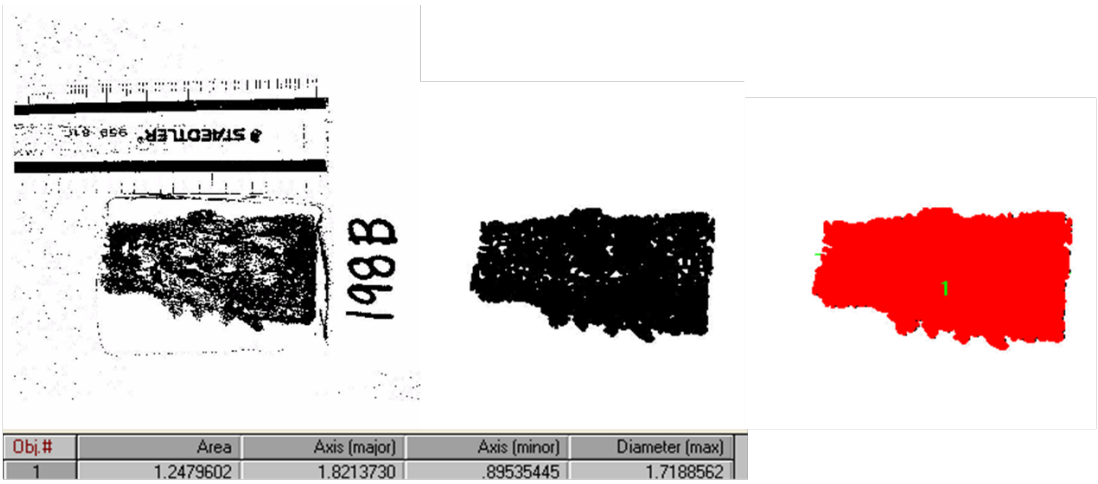


Figure 9. A series of pictures demonstrating the spall image processing and analysis to obtain the spall area. The “l” area in the figure is in square inches, while the other three measurements are in inches

# CHAPTER IV

# RESULTS AND DISCUSSION

## 4.1 Bearing Inner Rings (Cones)

In Figure 10 the cone spall areas are plotted against the total distance traveled during operation. The total distance traveled refers to the absolute total distance the bearing ran after the initiation of a spall, which includes both loaded (full-load) and unloaded (empty railcar) operating conditions. The data for this figure was divided into two spall size dependent growth regimes with spalls with areas above 6.45 $cm^2$ (1 $in^2$) and spall areas below 6.45 $cm^2$ represented by different data markers. A horizontal line was plotted at a spall area of 6.45 $cm^2$ (1 $in^2$). Based on data plotted in Figure 10, the cone spall area grows linearly ($R^2 = 0.86$) as a function of the distance traveled for spall sizes above 6.45 $cm^2$. As for the cone spall sizes below 6.45 $cm^2$, the data is more scattered which is reflected by the lower coefficient of determination ($R^2 = 0.38$) for the linear correlation. An explanation for these trends is that when the cone spall area is larger than 6.45 $cm^2$ (1 $in^2$), it tends to span the entire width of the cone raceway as seen in Figure 8; hence, growth is less scattered and correlates better with total distance traveled during operation.

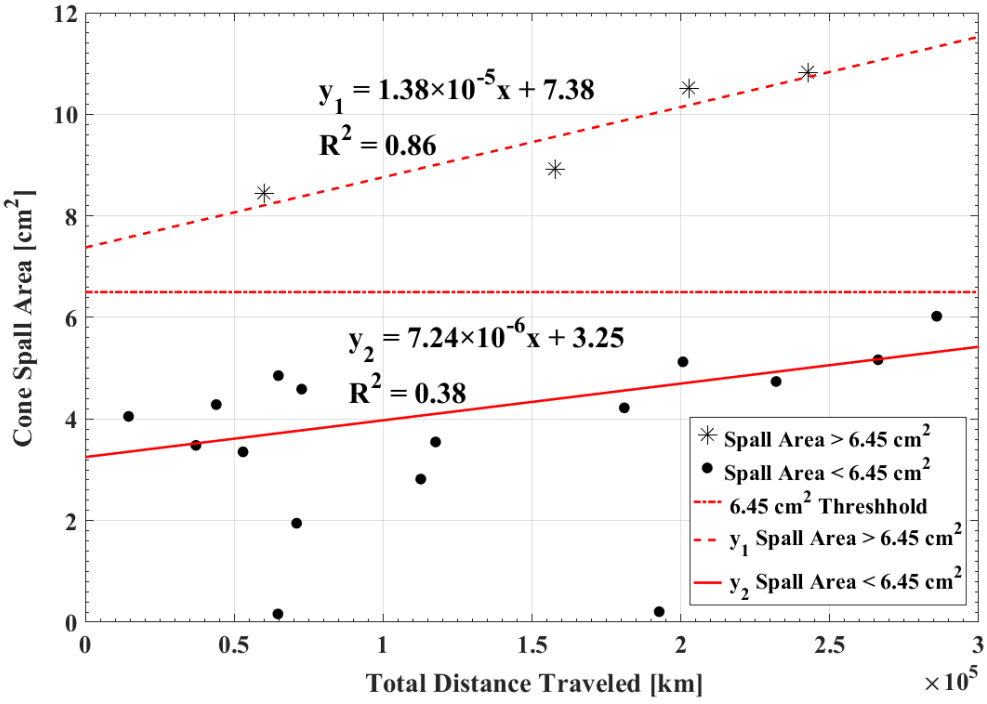


Figure 10. Cone spall area versus total distance traveled since spall initiation

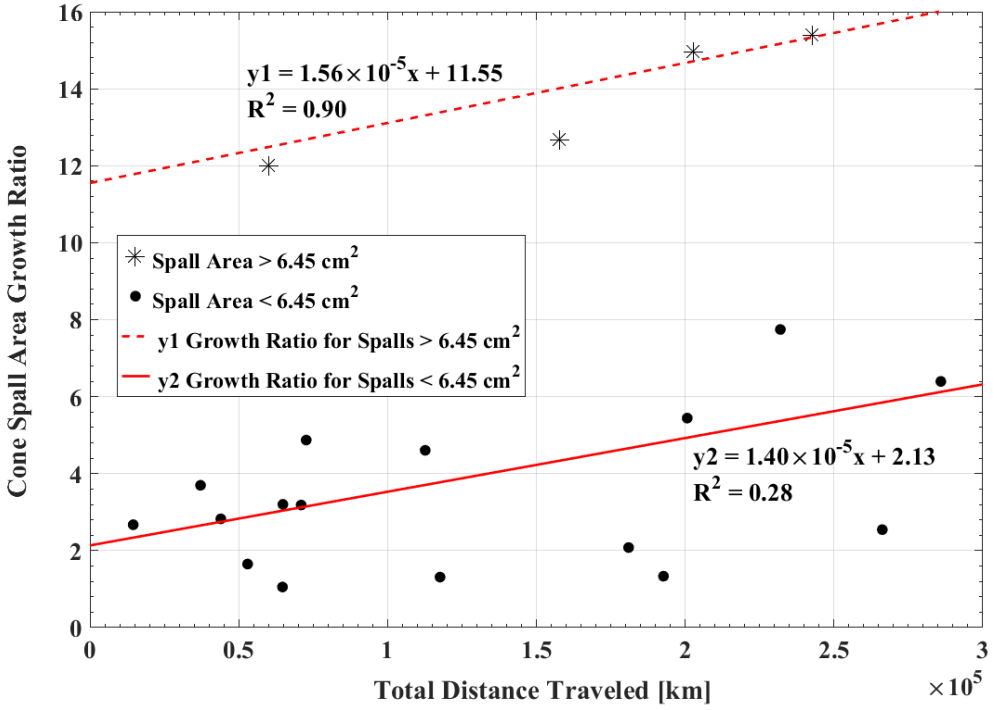


Figure 11. Cone spall area growth ratio versus total distance traveled

The spall area growth ratio is defined as the ratio of the current spall size to that of the original spall size that initiated on the rolling raceway. Figure 11 presents the cone spall area growth ratio as a function of the total distance traveled. The results similar to Figure 10, with two growth regimes indicated by the data points. The two trends in this figure are a representation of cone spalls sizes above and below 6.45 $cm^2$ (1 $in^2$). The linear correlation corresponding to $y_1$ represents the trend for the spalls that have areas above 6.45 $cm^2$, meanwhile, the linear correlation of $y_2$ represents the trend for spalls with areas below 6.45 $cm^2$. It can be observed from Figure 10 and Figure 11 that the slope in the correlation for cone spall areas above 6.45 $cm^2$ has a steeper trend than that of the correlation for spall areas below 6.45 $cm^2$. Meaning that there is a fundamental change in mechanism that is driving growth at a spall area of 6.45 $cm^2$, so that the spall growth accelerates. A possible explanation for this observation is the fact that tapered roller bearing spalls will tend to grow along the width of the rolling raceway until they reach the edges. When the spall has bridged the entire raceway, it begins to grow laterally along the raceway. However, if the shoulders of the raceway have not spalled, then the penetration into the spalled area will increase. This growth pattern can be observed in both inner (cone) and outer (cup) rings as seen in Figure 12 and Figure 13, more of these examples are available in Appendix A. An additional explanation for the rapid growth of spalls above the 6.45 $cm^2$ threshold is the fact that as the spall area increases, so does the sliding area, which causes the vibration levels within the bearing to intensify yielding faster degradation [7].


Figure 12. Cone spall growth pattern

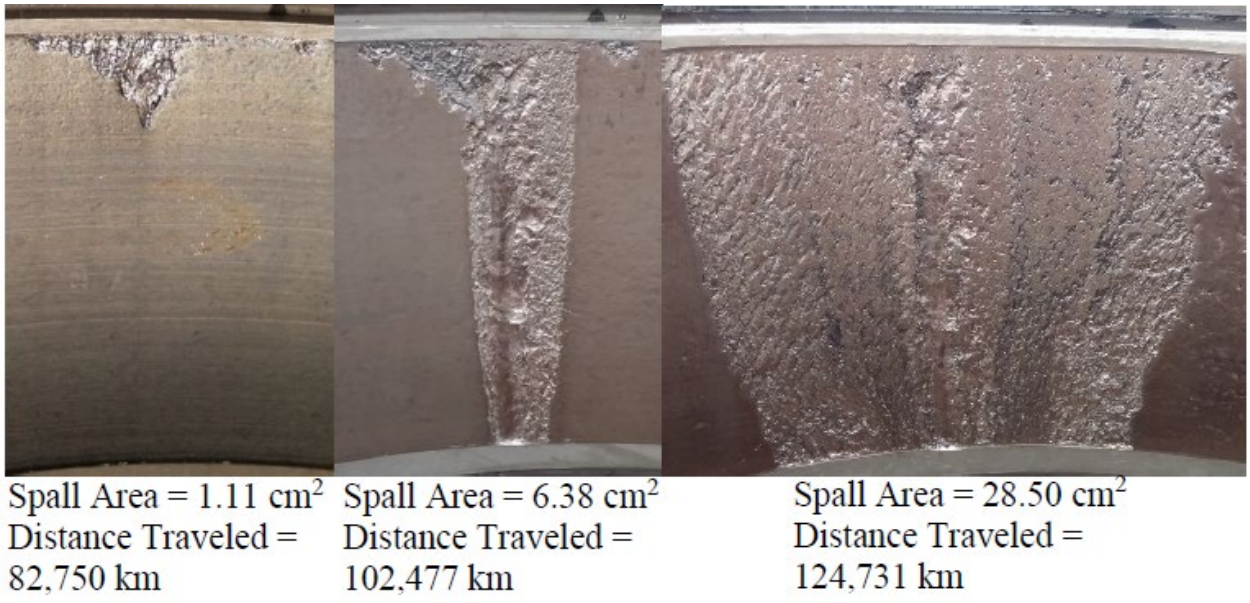


Figure 13. Cup spall growth pattern

The spall area growth rate is defined as the difference between the current spall size and the original spall size divided by the total distance traveled leading to the current spall size from the initial spall size. The cone spall area growth rate as a function of total distance traveled during operation is depicted in Figure 14. This figure again shows two trends that emerge for spall sizes with areas above and below 6.45 $cm^2$ (1 $cm^2$). Both trends indicate an exponential decay with high $R^2$ values. This indicates that the high initial growth rate for each regime exponentially decreases with distance traveled. The presence of this deceleration of spall growth indicates that an inherently conservative model of spall growth is easily achieved if the early growth, higher rate values are used in model development.

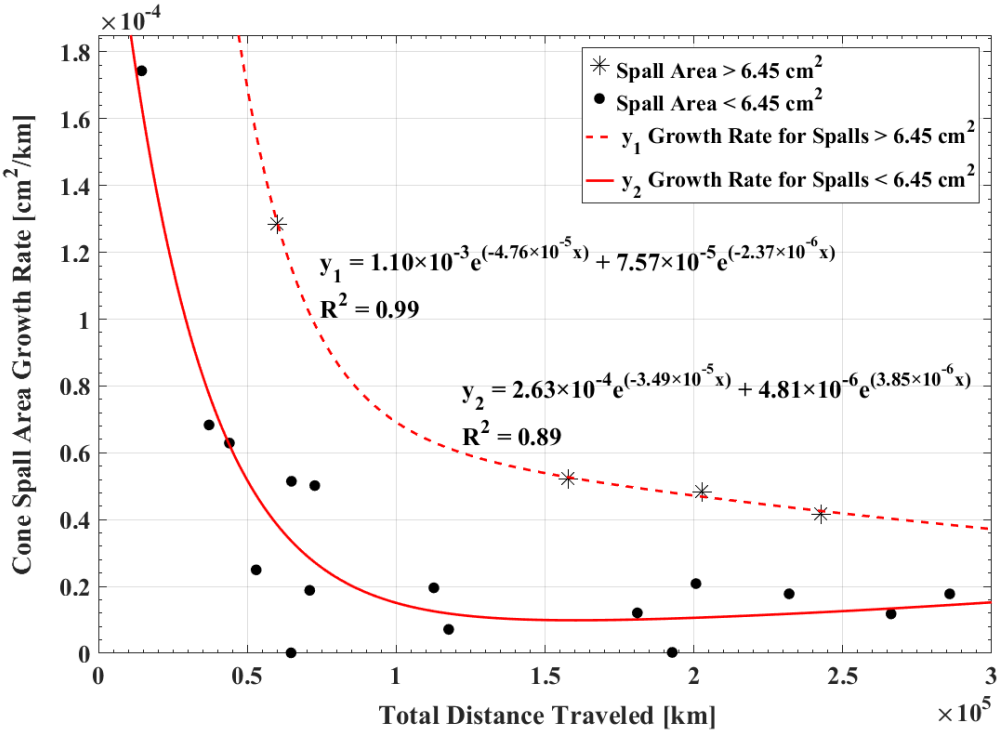


Figure 14. Cone spall area growth rate versus total distance traveled

Table 2 presents the inner ring (cone) spall area growth rate maximum, minimum, and average values. The values in the table were divided into two categories; cone spall areas less than and greater than 6.45 $cm^2$ (1 $in^2$). The average growth rate values for cone spalls, as shown in Table 2, are consistent with those previously discussed in that cone spall sizes above 6.45 $cm^2$ (1 $in^2$) will propagate at a faster pace than the cone spall areas that are below 6.45 $cm^2$. Furthermore, the results presented in Figure 14 and Table 2 indicate that a conservative maintenance schedule which removes at-risk bearings will not need to require service disruption as soon as a spall is detected. Regardless of spall size, growth will slow rather than accelerate so use of a single value for expected growth rate will still provide a very conservative estimate of remaining bearing life. Even those conservative estimates still provide a very large window for safe removal of a failing bearing. For example, consider the maximum observed growth rate of $1.28\times10^{-4}$ $cm^2$/km. Were this rate to be constant (rather than decreasing as observed), it would take about 1,090,000 km of operation for an initial cone spall to grow to 50% of the cone raceway surface area. It is important to remember that for a class F or class K railroad bearing, the inner ring (cone) raceway surface area is roughly 279 $cm^2$ (43 $in^2$), whereas, the outer ring (cup) has a raceway surface area of about 367 $cm^2$ (57 $in^2$) per raceway. Even if train operators or railcar owners chose a more conservative estimate for the residual service life of the bearing with a cone spall, let us say by taking 50% of the calculated operation distance, it will still allow an ample timeframe for railcar owners to plan for wheel-set replacement with minimal disruption to operations.

Table 2. Cone and cup spall area growth rate values

| | Spall Size | Average Growth Rate $[cm^2/km]\times10^{-4}$ | Maximum Growth Rate $[cm^2/km]\times10^{-4}$ | Minimum Growth Rate $[cm^2/km]\times10^{-4}$ |
|---|---|---|---|---|
| Cone (Inner Ring) | $< 6.45\ cm^2$ ($1\ in^2$) | 0.35 | 1.74 | 0.001 |
| | $> 6.45\ cm^2$ ($1\ in^2$) | 0.68 | 1.28 | 0.42 |
| Cup (Outer Ring) | $< 12.9\ cm^2$ ($2\ in^2$) | 1.01 | 3.83 | 0.07 |
| | $> 12.9\ cm^2$ ($2\ in^2$) | 3.41 | 6.52 | 1.09 |

### 4.2 Bearing Outer Rings (Cups)

The cup spall area plotted against the total distance traveled during operation is depicted in Figure 15. The data presented in this figure exhibits similar behavior to that of Figure 10 for the cone spall area; however, the threshold between the two categories seems to be at 12.9 $cm^2$ (2 $in^2$) spall area. From Figure 15, two linear correlations are displayed, one for cup spall areas above 12.9 $cm^2$ with a coefficient of determination ($R^2$) value of 0.81, and a second correlation for cup spall areas below 12.9 $cm^2$ with a lower $R^2$ value of 0.34. Just like the case with the cone spalls, the slopes of the two linear correlations displayed in Figure 15 propose a faster growth rate for spall areas above 12.9 $cm^2$. As previously stated, once the spall propagates across the width of the raceway, it will begin to rapidly grow along the raceway circumference, as seen in Figure 12 and Figure 13. The fact that the threshold for the outer rings (cups) is 12.9 $cm^2$ as opposed to 6.45 $cm^2$ for the inner rings (cones) is explained hereafter.

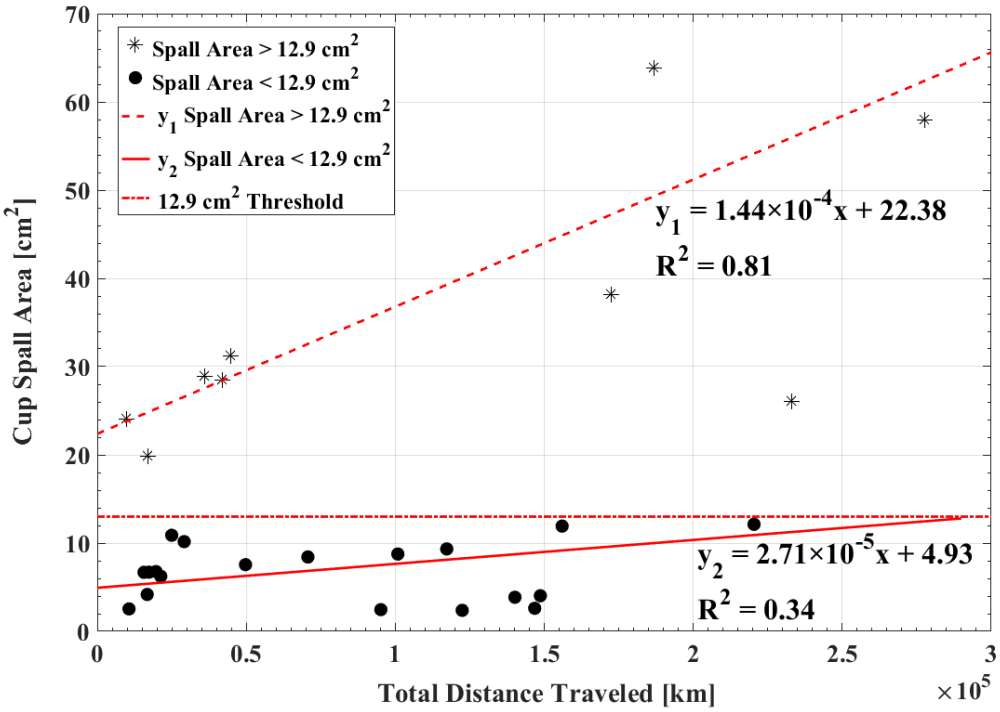


Figure 15. Cup spall area versus total distance

It is important to understand that the threshold areas of 12.9 $cm^2$ (2 $in^2$) corresponding to the outer rings and 6.45 $cm^2$ (1 $in^2$) for the inner rings (cones) are empirical and were noticed when the data points were plotted. The following hypothesis were made regarding these thresholds. Form Figure 16, it can be seen that the projected area of a roller on the cup raceway is roughly 11.68 $cm^2$ (1.81 $in^2$). Since the spall shape varies, it is likely that a spall area approximating the projected area of the roller is enough to allow the roller to completely enter the defect depression, as seen in Figure 17, and engage with the spall shoulder with a high enough lateral load as opposed to vertical contact pressure. As a result of this, the subsurface shear stress below the shoulder will increase, thus, increasing the rate of growth. In cone spalls, the 50% smaller area threshold is possibly due to the convex surface of the cone which allows the rollers to achieve significant lateral engagement with the shoulder of the spall at a smaller defect area. This results in roughly 10% higher subsurface Hertzian shear stress. Though the

cone is rotating, and the spall spends part of its time outside the loaded region, the cone will still pass through the most heavily-loaded point on the bearing with every cycle.

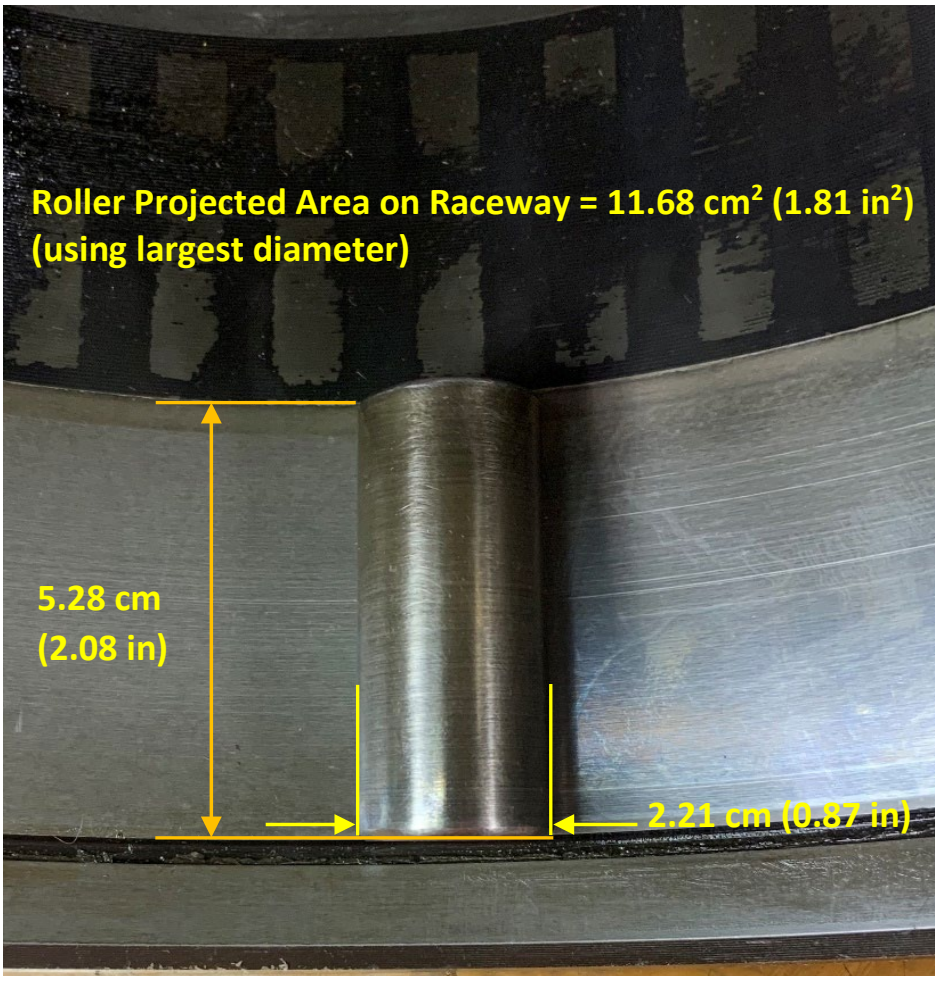


Figure 16. Projected area of a roller on the outer ring (cup) raceway

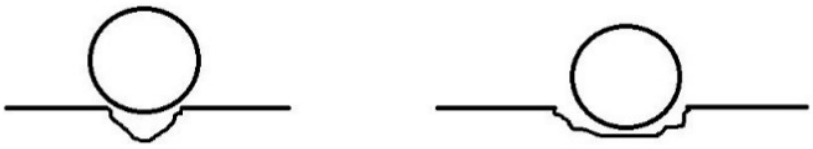

Figure 17. Roller defect depression

On average, spall initiation will take much longer than spall propagation. When the raceway begins to pit, the initial spalling originates and will rapidly accelerate the spall propagation. In general, the spalls in both cups and cones will tend to spread across the width of the raceways first before initiating growth along the raceway circumference. Consequently, as the spall reaches a specific size, spall growth will noticeably accelerate with total distance traveled during operation. This trend is also reflected in Figure 18 which gives the cup spall growth ratio versus the total distance traveled. In Figure 18, the data shows the cup spall growth ratio increasing exponentially after 160,000 km of operation. Note that the circled data point in Figure 18 and Figure 19 is an outlier and was not used to formulate the correlations provided in the figures. The associated bearing was one with uncharacteristically bad quality steel that contained many subsurface inclusions and impurities. This bearing would have been caught by the manufacturer's quality control procedures and would not have been allowed to be sold into service.

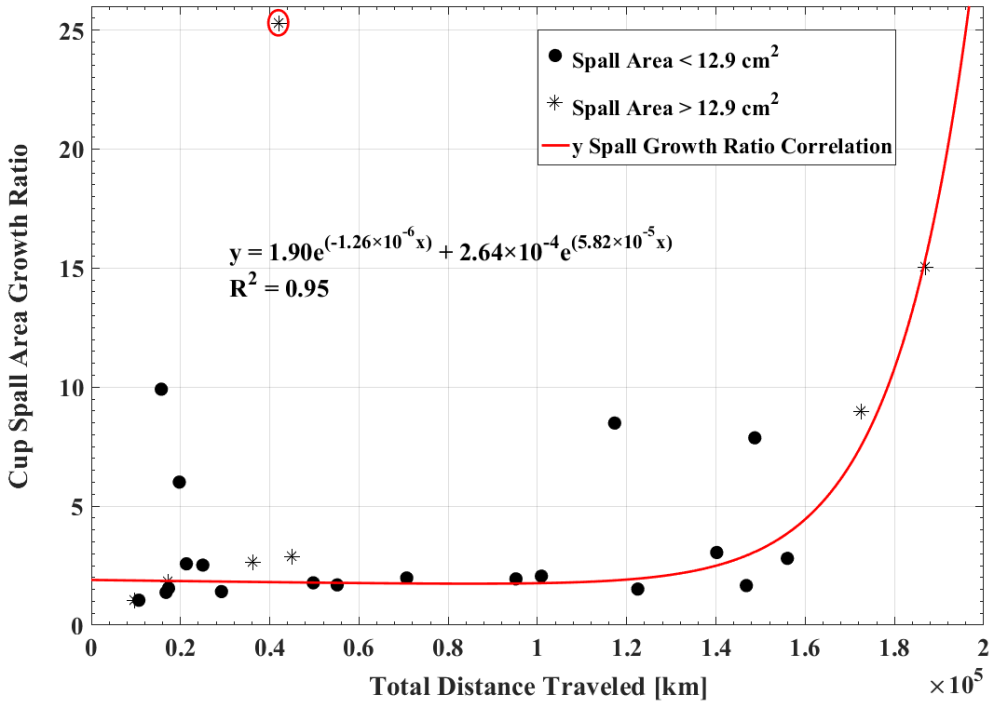


Figure 18. Cup spall area growth ratio versus total distance traveled since initiation

The cup spall area growth rate in [$cm^2$/km] as a function of total distance traveled during operation is given in Figure 19. As previously stated, spall growth is mainly affected by the raceway boundaries. Looking at Figure 19, it can be seen that the cup spall area growth rate starts high as the spall initiates and rapidly propagates, however, when the spall reaches the raceway boundaries it begins to slow down. This behavior is presented in the $y_2$ growth rate relation of Figure 19 for cup spall areas less than 12.9 $cm^2$. Continuous operation will allow for the spall to spread across the width of the raceway, thus, the cup spall area growth rate will considerably increase as the spall begins to propagate along the circumference of the raceway unhindered but will slow down as the cup spall area moves away from the fully-loaded region. This effect is demonstrated by the growth relation in $y_1$ of Figure 19 for cup spalls with areas greater than 12.9 $cm^2$.

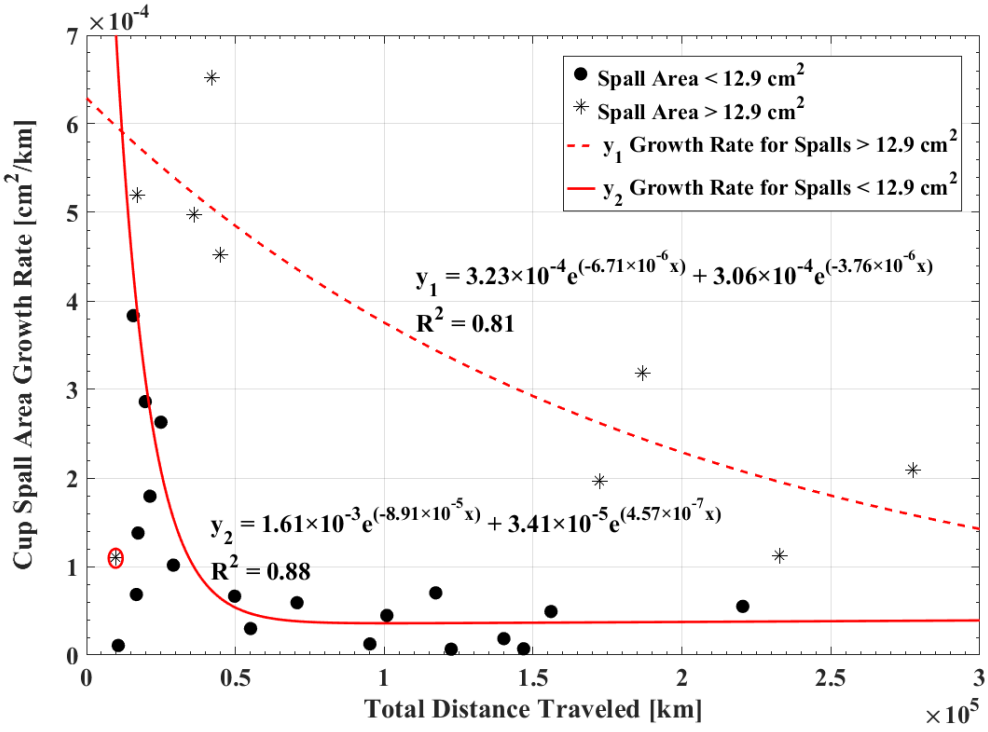


Figure 19. Cup spall area growth rate versus total distance traveled since initiation

Table 2 also provides the cup spall area growth rate maximum, minimum, and average values. These values were split into two categories; cup spall areas less than and greater than 12.9 $cm^2$ (2 $in^2$). Note that the growth rate values for cup spall areas above 12.9 $cm^2$ are greater than those for cup spall areas below 12.9 $cm^2$. More importantly, in comparison to the values for cones, it is apparent that the cup spalls will grow significantly faster. It is unlikely that the rate difference is due to major differences in the mechanics since the contact stresses between the roller and the cone should be higher than those for a roller against the cup. The difference in rate can perhaps be due to the railroad bearing operation. In rail service, the bearing outer ring (cup) remains stationary while the bearing inner rings (cones) rotate synchronously with the axle and wheels, undergoing cyclic loading and unloading as they enter and exit the loaded and unloaded zones. As per the laboratory setup used in this study, the cup spalls were placed directly under

the applied load, so they were never unloaded during bearing operation. The experiments conducted in the laboratory represent worst-case loading for a cup spall and cannot occur on cone spalls since they rotate with the cone. Therefore, each cup spall sees many more roller impacts per kilometer of operation than a spall on a rotating cone will experience.

Finally, just like in the example for cone spalls, if the maximum growth rate of $6.52\times10^{-4}$ $cm^2/km$ is assumed, and starting with a spall of insignificant size, it would take 281,000 km of operation for a cup spall to propagate to 50% of the cup raceway surface area (367 $cm^2$ or 57 $in^2$). It is safe to say that for both cone and cup spalls the railcar operators have sufficient time to schedule bearing replacement during an ordinary yard stop between ladings.

# CHAPTER V

# CONCLUSIONS

The study summarized in this thesis represents ongoing work that started in 2010 for tracking spall propagation in bearing inner (cones) and outer (cup) rings with distance traveled during operation. In previous work done by the University Transportation Center for Railway Safety (UTCRS) [18], [19], the authors presented initial data and preliminary models that described the spall size growth as a function of distance traveled for railroad bearings. The previous publications modeled the work done for inner (cone) rings and outer (cup) rings, separately; whereas, this thesis presents refined models based on a larger dataset for cone and cup spall growth as a function of distance traveled.

Several conclusions can be drawn from the data. First, spall size in both cups and cones has a distinct effect on the growth rate of the defect. In both cases, once the spall initiates on the raceway, the defect will grow perpendicular to the rolling direction and continue to spread across the raceway until the boundaries are reached. From that point on, the spall will propagate along the raceway circumference with distance traveled. Second, in cones, it is observed that the spall growth rate will increase with spall size, while for cup spalls, the growth rate will decrease as edges of the spall move out of the fully-loaded zone of the bearing. Thirdly, there is an apparent threshold spall area where the growth rate transitions to higher rates. The thresholds identified in this study are 6.45 $cm^2$ (1 $in^2$) for cone spalls, and 12.9 $cm^2$ (2 $in^2$) for cup spalls.

These threshold areas are likely related to the contact surface areas, when the bearing is under full-load conditions, between the roller and cone and cup. Spalls larger than these sizes will consistently permit the roller to fully enter the spall depression and interact with the shoulders of the spall with a larger lateral component which has a greater effect on subsurface shear and, thus, spall growth rate.

From the spall area growth rate results presented in this thesis, it is evident that the spalls will grow at a much faster rate in bearing outer rings (cups) than in bearing inner rings (cones). This finding can partially be explained by the fact that, for the most part, cups are fixed and rollers entering the spall will always be under load if the spall is in the loaded zone, however, cones rotate in and out of the loaded region and so a spall will equally divide its time between the loaded and unloaded zones of the bearing and will spend only a small fraction of its life in the region of maximum load. Therefore, it is crucial to identify whether the spall has initiated on the cup or the cone to accurately predict the spall growth trend. The bearing condition-monitoring algorithm that was developed by the UTCRS research team can accurately identify the location of the spall initiation, and the vibration levels within the bearing can be used to approximate the relative size of the spall so the appropriate spall prognostics models can be applied.

Both the cone and the cup growth rate models presented in this study exhibit a similar behavior. The trends demonstrate that the spall grows perpendicularly at a fairly high rate but will decrease its growth rate as the spall reaches the raceway boundaries. After the spall has propagated across the entire width of the raceway, it will begin to expand along the raceway

circumference with an initial fast growth rate that will decrease as the edges of the spall move out of the region of the fully-loaded zone.

In conclusion, the consistent behavior of spall propagation in railroad bearings, even under varying conditions such as load, speed, and temperature, suggest that a simple empirical model of spall growth can serve as a foundation for predicting conservative residual life in a bearing when a spall is detected. If coupled with an advanced bearing condition monitoring algorithm that detects the beginning of spall formation, location, and approximate size, it can be utilized in scheduling economical and proactive maintenance cycles that will minimize the unnecessary and costly train stoppages and delays while preventing disastrous train derailments due to bearing failures.

Appendix A

Appendix A

Spall Progression

Spall Area = 4.24 $cm^2$
Distance Traveled = 37,631 km

Spall Area = 11.92 $cm^2$
Distance Traveled = 193,622 km

Spall Area = 38.13 $cm^2$
Distance Traveled = 210,140 km

Spall Area = 1.26 $cm^2$
Distance Traveled = 14,450 km

Spall Area = 2.46 $cm^2$
Distance Traveled = 109,620 km

Spall Area = 23.22 $cm^2$
Distance Traveled = 154,608 km

Spall Area = 12.13 cm² Spall Area = 26.09 cm² Spall Area = 57.97 cm²

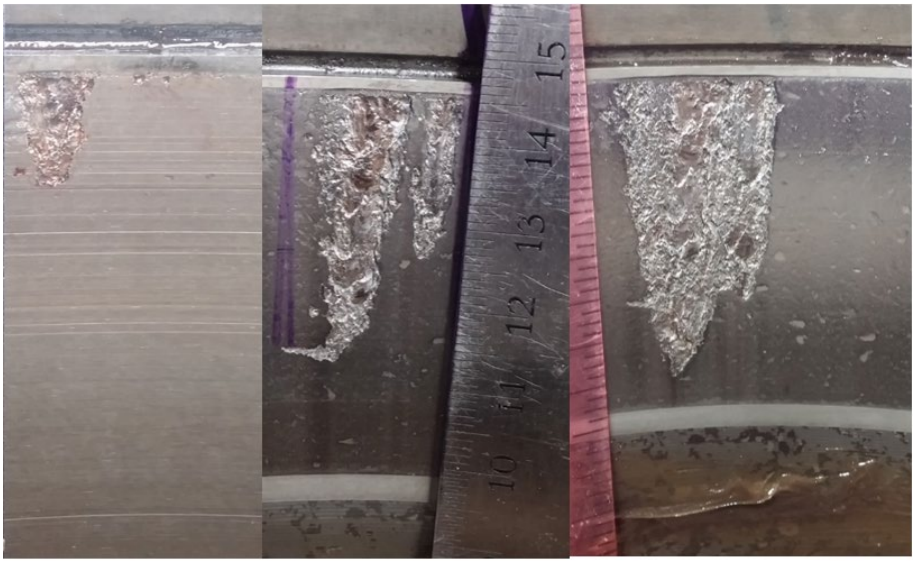


Spall Area = 0.63 cm²
Distance Traveled = 208,746 km

Spall Area = 4.11 cm²
Distance Traveled = 298,058 km

Spall Area = 7.88 cm²
Distance Traveled = 305,733 km

Spall Area = 1.11 $cm^2$
Distance Traveled = 82,750 km

Spall Area = 6.38 $cm^2$
Distance Traveled = 102,477 km

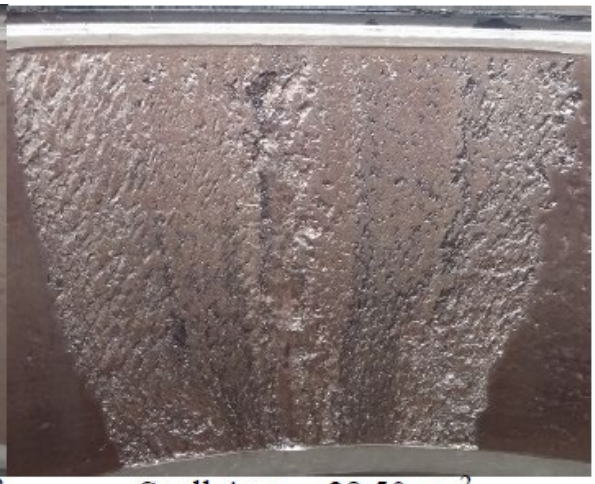

Spall Area = 28.50 $cm^2$
Distance Traveled = 124,731 km

Spall Area = 8.92 $cm^2$
Distance Traveled = 477,437 km

Spall Area = 10.50 $cm^2$
Distance Traveled = 522,502 km

Spall Area = 10.85 $cm^2$
Distance Traveled = 562,552 km

Spall Area = 3.48 $cm^2$
Distance Traveled =
443,556 km

Spall Area = 4.59 $cm^2$
Distance Traveled =
479,061 km

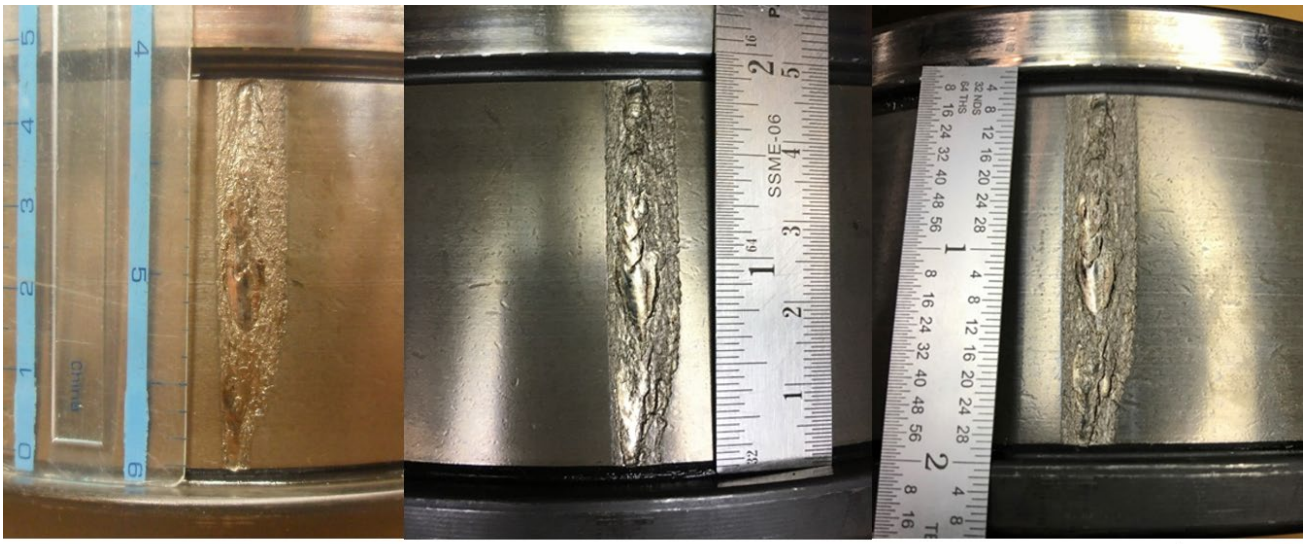

Spall Area = 4.05 $cm^2$
Distance Traveled =
420,935 km

Spall Area = 4.28 $cm^2$
Distance Traveled =
450,381 km

Spall Area = 4.85 $cm^2$
Distance Traveled =
471,236 km

Spall Area = 0.61 $cm^2$
Distance Traveled = 119,901 km

Spall Area = 2.88 $cm^2$
Distance Traveled = 232,554 km

Spall Area = 5.04 $cm^2$
Distance Traveled = 351,870 km

# REFERENCES


[1] SKF: Bearing designs, tapered roller bearing units. Extract from the Railway technical handbook, vol. 1, p. 76–87. [chapter 4].

[2] Tarawneh, C., Turner, J. A., Wilson, B. M., and Koester, L. (2013), "Service Life Testing of Railroad Bearings with Known Subsurface Inclusions Detected with Advanced Ultrasonic Technology," Int. J. of Railway Technology, 2(3), pp 55-78.

[3] Sadeghi, F., Jalalahmadi, B., Slack, T. S., and Raje, N. K. (2009), "A Review of Rolling Contact Fatigue," ASME Journal of Tribology, 131(4), 041403. DOI: 10.1115/1.3209132

[4] Tarawneh, C., Koester, L., Fuller, A. J., Wilson, B. M., and Turner, J. A. (2012), "Service Life Testing of Components with Defects in the Rolling Contact Fatigue Zone," ASTM International, STP 1548, West Conshohocken, PA, pp 67-83.

[5] Wilson, B. M., Fuller, A. J., Tarawneh, C., and Turner, J. A. (2016), "Near Race Inclusions in Bearing Components and the Resultant Effect on Fatigue Initiation and Component Life," Proceedings of the Conference on Railway Excellence (CORE), Melbourne, Australia.

[6] Nikas, G. K. (2016), "Algebraic Equations for the Pile-Up Geometry in Debris Particle Indentation of Rolling Elastohydrodynamic Contacts," ASME Journal of Tribology, 138(2), 021503. DOI: 10.1115/1.4031516

[7] Goshima, T., Ishihar, S., Shimizu, M., and Mizoguchi, A. (2010), "Crack Propagation and Initiation Lives for Surface Pitting Due to Rolling/Sliding Contact," Journal of Thermal Stresses, 33(11), pp 1087-1106. DOI: 10.1080/01495739.2010.511917

[8] Gonzalez, A., Tarawneh, C., Wilson, B. M., and Turner, J. A. (2015), "Tracking of Spall Deterioration on Tapered Roller Bearing Raceways," Proceedings of the ASME Joint Rail Conference, San Jose, CA.

[9] Li, Y., Billington, S., Zhang, C., Kurfess, T., Danyluk, S., and Liang, S. (1999), "Dynamic Prognostic Prediction of Defect Propagation on Rolling Element Bearings," Tribology Transactions, 42(2), pp 385-392.

[10] Qian, Y., Yan, R., and Gao, R. X. (2017), "A Multi-Time Scale Approach to Remaining Useful Life Prediction in Rolling Bearing," Mechanical Systems and Signal Processing, 83, pp 549-567. https://doi.org/10.1016/j.ymssp.2016.06.031

[11] Zhou, Q., Xie, L., Jin, X., Wang, Z., Wang, J., Keer, L. M., and Wang, Q. (2014), "Numerical Modeling of Distributed Inhomogeneities and Their Effect on Rolling-Contact Fatigue Life," ASME Journal of Tribology, 137(1), 011402. DOI: 10.1115/1.4028406

[12] Liu, H., Liu, H., Zhu, C., He, H., and Wei, P. (2018), "Evaluation of Contact Fatigue Life of a Wind Turbine Gear Pair Considering Residual Stress," ASME Journal of Tribology, 140(4), 041102. DOI: 10.1115/1.4039164

[13] Wilson, B. M., Fuller, A. J., Tarawneh, C., and Turner, J. A. (2015), "Early Bearing Fatigue Initiation by the Identification and Selection of Bearings with Near Race Defects," Proceedings of the International Heavy Haul Association Conference, Perth, Australia.

[14] Tarawneh, C., Sotelo, L., De Los Santos, N., Villarreal, A., Lechtenberg, R., and Jones, R. (2016), "Temperature Profiles of Railroad Tapered Bearings with Defective Inner and Outer Rings," Proceedings of the ASME Joint Rail Conference, Columbia, SC.

[15] Montalvo, J., Tarawneh, C., and Fuentes, A. (2018), "Vibration-Based Defect Detection for Freight Railcar Tapered-Roller Bearings," Proceedings of the ASME Joint Rail Conference, Pittsburgh, PA.

[16] Tarawneh, C., Ley, J., Blackwell, D., Crown, S., and Wilson, B. M. (2018), "Onboard Load Sensor for Use in Freight Railcar Applications," Int. J. of Railway Technology, in press.

[17] De Los Santos, N., Jones, R., Tarawneh, C., and Villarreal, A. (2017), "Development of Prognostic Techniques for Surface Defect Growth in Railroad Bearing Rolling Elements," Proceedings of the ASME Joint Rail Conference, Philadelphia, PA.

[18] De Los Santos, N., Jones, R., Tarawneh, C., and Fuentes, A. (2018), "Defect Prognostic Models for Spall Growth in Railroad Bearing Rolling Elements," Proceedings of the ASME Joint Rail Conference, Pittsburgh, PA.

## BIOGRAPHICAL SKETCH

Nancy De Los Santos was born in Mission, Texas on August 23, 1993. She attended Pharr-San Juan-Alamo High School and graduated in the Spring of 2011. Afterwards, she attended the University of Texas Rio Grande Valley, where she graduated with her bachelor's degree in Mechanical Engineering in the Spring of 2016. She later chose to continue her studies at the University of Texas Rio Grande Valley and obtained her Master of Science degree in Mechanical Engineering in July 2019. Nancy may be reached by email at ndelossantos.93@gmail.com.